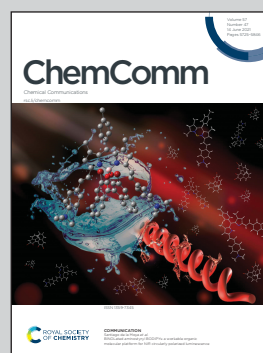**Showcasing research from Sekine's Laboratory/ Department of Applied Chemistry, Waseda University, Tokyo, Japan**

Enhanced activity of catalysts on substrates with surface protonic current in an electrical field – a review

The surface protonic conductivity on porous semiconductor ceramic supports enhances catalytic activity for various reactions involving hydrogen-containing reactants. We summarize the electrical enhancement and how it enhances yield and lowers reaction temperatures of industrially important chemical processes.

ROYAL SOCIETY OF CHEMISTRY

rsc.li/chemcomm

Registered charity number: 207890

ChemComm

FEATURE ARTICLE

Enhanced activity of catalysts on substrates with surface protonic current in an electrical field – a review

Yudai Hisai,[a] Quanbao Ma,[b] Thomas Qureishy,[c] Takeshi Watanabe,[d] Takuma Higo, [iD][a] Truls Norby*[b] and Yasushi Sekine [iD]*[a]

It has over the last few years been reported that the application of a DC electric field and resulting current over a bed of certain catalyst-support systems enhances catalytic activity for several reactions involving hydrogen-containing reactants, and the effect has been attributed to surface protonic conductivity on the porous ceramic support (typically ZrO_2, CeO_2, $SrZrO_3$). Models for the nature of the interaction between the protonic current, the catalyst particle (typically Ru, Ni, Co, Fe), and adsorbed reactants such as NH_3 and CH_4 have developed as experimental evidence has emerged. Here, we summarize the electrical enhancement and how it enhances yield and lowers reaction temperatures of industrially important chemical processes. We also review the nature of the relevant catalysts, support materials, as well as essentials and recent progress in surface protonics. It is easily suspected that the effect is merely an increase in local *vs.* nominal set temperature due to the ohmic heating of the electrical field and current. We address this and add data from recent studies of ours that indicate that the heating effect is minor, and that the novel catalytic effect of a surface protonic current must have additional causes.

[a] *Department of Applied Chemistry, Waseda University, Tokyo 169-8555, Japan. E-mail: ysekine@waseda.jp*
[b] *Department of Chemistry, Centre for Materials Science and Nanotechnology, University of Oslo, FERMiO, Gaustadalléen 21, NO-0349 Oslo, Norway.*
  E-mail: truls.norby@kjemi.uio.no
[c] *Department of Chemistry, Hylleraas Centre for Quantum Molecular Sciences, University of Oslo, P.O. Box 1033 Blindern, NO-0315 Oslo, Norway*
[d] *SPring-8, JASRI, 1-1-1, Koto, Sayo, Hyogo, 679-5198, Japan*

Truls Norby

Truls Norby (b. 1955), PhD from University of Oslo (UiO) 1986, became professor at the Department of Chemistry UiO 1994 and since 1997 has headed the Group for Electrochemistry. He works with defects and transport in materials for solid-state fuel cells, electrolysers, batteries, membranes, and sensors, specialising in protons and protonic transport in oxides and on their surfaces. Norby has published 275 journal papers, graduated >100 Master- and PhD-students, and is a member of the Norwegian Academy of Science and Letters and other national academies. He has founded 4 companies, won the UiO Innovation Prize 2012 and the Norwegian Guldberg-Waage medal for chemistry 2018.

Yasushi Sekine

Yasushi Sekine (b. 1968), PhD from The University of Tokyo 1998, became professor at the Department of Applied Chemistry, Waseda University in 2012. He works with low temperature catalysis, specialising in protons and protonic transport in oxides and on their surfaces. Sekine has published 202 journal papers, supervised 96 Master- and 11 PhD-students, and is a fellow of the RSC (FRSC) and a member of other national academies.

Many important and large-scale chemical reactions are carried out efficiently by means of catalysts to limit temperature, footprint and cost, and increase yield and reactor lifetime. The need to incorporate renewable energy into chemical reactions is gaining importance, such as operation of on-demand chemical reactions at relatively low temperatures. Non-equilibrium plasmas, photochemical, photoelectrochemical, and electrochemical reactions (electrosynthesis) as well as catalytic reactions with the application of electric fields and currents have been proposed as means of realizing such on-demand chemical reactions.

Through the development and study of systematic methodologies for a number of heterogeneous catalytic reactions, it has been found that the application of electric fields and small currents to various metal catalysts on ceramic semiconducting supports can significantly enhance the reaction rates.[1–20] Also, non-equilibrium electrocatalytic processes include non-faradaic electrochemical modification of catalytic activity (NEMCA)[21–25] and reactions in plasmas and electrical discharges[26–33] have been proposed. NEMCA works at rather higher temperatures thanks to the oxygen anion migration in the oxide by the application of an electric field. Plasma-aided catalytic reactions have been attracting much attention recently, but it requires a high electrical energy consumption and it is difficult to maintain a stable catalyst structure. Compared to these processes, the catalytic effect of the electric field appears to be operative and maintaining high yields and selectivity and hence cost efficiency of various chemical reactions at low temperatures. Activation of catalysts by the application of an electric field evidently results from the migration of protons on the surface of the catalyst support and their interaction with reactant molecules such as N_2, CO_2, and CH_4 at the catalyst support–metal interface.[1,2,34–44] We have studied several reactions and catalysts and used a wide range of techniques to demonstrate the general principle of catalytic activation and to clarify the mechanism. Regarding the effect of electric fields (denoted as "EF") on reactions, it was found that the apparent activation energy of the reaction is greatly reduced.

Here, we summarize the fundamentals, applications, theories, and developments of catalytic reactions in the electric field to help further research and development. In addition, as a means of applying the reaction to a wide variety of applications, examples of its application to ammonia synthesis, hydrogen and syngas production (steam reforming, dry reforming), hydrocarbon dehydrogenation, carbon dioxide activation, etc. will be introduced in detail, and the reaction mechanism will be summarized to provide a roadmap for further energy efficiency improvement. In laboratory demonstrations so far, the electrical energy required is relatively high for exothermic reactions including ammonia synthesis. For instance typically 1 kW h per kg NH_3 synthesized from $N_2 + 3H_2$ is required for ammonia synthesis, and this needs to be reduced by at least an order of magnitude at scale-up if the EF enhanced catalysis is to be viable, as such requiring that the enhancement is not by ohmic Joule heating. On the other hand, the energy efficiency is

rather high, about ~70% on the endothermic reactions including reverse water gas shift, hydrogen evolution from methylcyclohexane, steam/dry reforming of hydrocarbons or alcohols.

General description and considerations

Here we first provide an introductory overview of the general principles and approaches.

The catalysts

For heterogeneous catalysts, which are reported to enable enhanced catalytic activity upon application of an electric field, ceramic supports with a relatively high bandgap (i.e., semiconducting) and negligible bulk electrical conductivity are important. By taking the form of powdered catalysts or porous ceramics and providing the surface with adsorbed species, the surface exhibits proton conduction by the Grotthuss mechanism. For this purpose, fluorite binary oxides such as CeO_2[34] and perovskites such as $SrZrO_3$[41,42] are good candidates. The choice of catalyst support should be considered based on its physical properties:[45] conductors such as Fe_2O_3 can sustain an electric current but do not promote catalytic activity, whereas insulators such as Al_2O_3 cannot sustain sufficient surface protonic current, and the electric field results only in discharge. Only semiconducting type supports such as CeO_2 and $SrZrO_3$ appear to satisfy the required physical properties: surface protonic conductivity is a key factor, but also the presence of redox-active cations and possibly electronic transport seem important. For preparing active catalysts, various active metals, such as Ru, Pt, Pd or Ni, which show high catalytic activity, are loaded on the support by an impregnation method. The supported metal catalyst is calcined at 673–973 K for 2–12 hours. After calcination, the solid is pressed and sieved into agglomerates of diameter 355–500 μm. The catalyst structure and composition are evaluated by X-ray diffraction (XRD) and surface area analysis using the Brunauer–Emmett–Teller (BET) method before and after activity tests under the electric field.

Reactor and temperature measurement

The structure of a typical reactor is shown in Fig. 1. It consists of a conventional fixed-bed flow reactor in a furnace and two electrodes for applying an electric field on the catalyst.[1,2] Usually, several hundred mg of catalyst is packed between the electrodes in the form of mesh or plates of Au or other materials, and the two electrodes are mounted vertically or coaxially on a fixed catalyst bed. A small current (a few mA) is applied to this catalyst bed at a DC voltage of 70–800 V. The stability of the voltage required for a given current is checked using a digital oscilloscope. The field strength in this process (on the order of 10^5 V m^{-1}) is intermediate between other methods such as NEMCA (10^3 V m^{-1})[46] and plasma
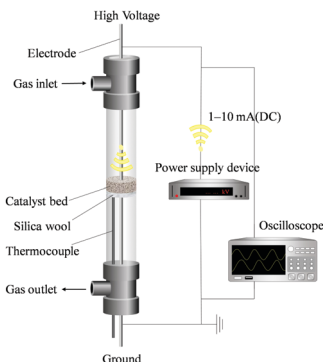
Fig. 1 Schematic image of the standard fixed-bed reactor.

$(>10^7 \text{ V m}^{-1})$.[47] The catalyst layer acts as a kind of solid electrolyte. A thermocouple is attached to the reactor to measure the temperature of the catalyst layer. The products released from the gas outlet are qualitatively and quantitatively analyzed using gas chromatography with flame ionization detector (GC-FID), gas chromatography with thermal conductivity detector (GC-TCD), quadrupole mass spectrometer (Q-Mass), or ion chromatography.[34,42]

When a weak electric current is applied to the catalyst bed by the electric field, Joule heat is generated, which may increase the temperature of the bed and the reaction rate. However, the power consumption by the field and current is low (typically 2 W, maximum 8 W) and the effect of the temperature rise of the catalyst bed on the reaction is small, confirmed by the thermocouple. Therefore, the induced Joule heat is estimated to be negligible in this process.[48,49]

Attempts to measure the catalyst temperature during the application of the electrical current in ammonia synthesis experiments have also been made in a setup at University of Oslo employing a ProboStat™ sample holder system (NORECS AS, Norway) with a wider quartz tube bed reactor equipped with Au mesh electrodes and taking up to 1 g catalyst. Thermocouples to the side of the quartz tube, in the exiting gas just under the frit, and in a protrusion of the quartz glass wall into the catalyst were used to more closely – yet still crudely – evaluate temperature effects. It was confirmed that application of 5 mA of current and typically 2 W of power caused temperature increases of only a few degrees at a nominal furnace and reactor temperature of 400 °C, increasing to typically 10 K at 200 °C and 20 K below 100 °C.

Rough calculations show that the gas flow can only absorb minute amounts of the ohmic heat, that radiation accounts for only a small fraction, and that heat conduction through the quartz walls to the surrounding reactor and furnace accounts for most of the heat transport, and indeed rationalizes the observed modest increase of only a few degrees.

For measuring and assuring the "real" catalytic temperature, we have evaluated it by *operando*-EXAFS comprising Debye–Waller factor analysis.[50] We measured Pd K-edge for PdO in samples of Pd catalyst on CeO$_2$ support with and without electrical field and current by EXAFS (BL14B2, SPring-8 at Hyogo, Japan) and compared with measurements of PdO samples at various
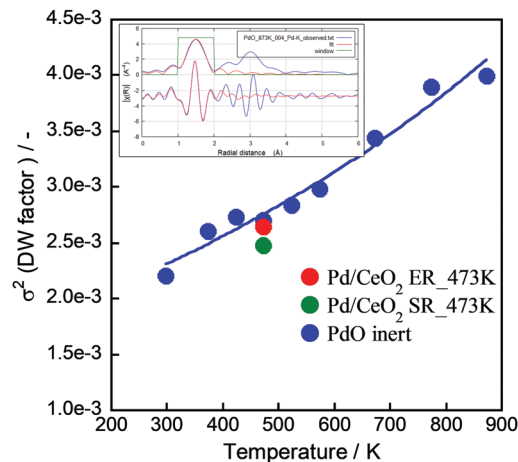

Fig. 2 Local heat evaluation using EXAFS. "ER" is a sample under the electric field and current, "SR" is without.

temperatures, see Fig. 2. The σ^2 value at 473 K with the electric field is a little larger than at 473 K without the electric field, but it does not exceed the value of PdO at 473 K (Fig. 2). If the difference is interpreted along the same slope as for the PdO sample, the electrical power leads to an increase of <50 K in the Pd catalyst. This means that the local heating effect by the electric field is rather small in the electric field over the catalyst of Pd/CeO$_2$.

Reaction mechanism

We have reported that by applying a DC electric field over the catalyst and conducting a small current, the catalytic activity is enhanced, the reaction proceeds at a much lower temperature than ever, and the apparent activation energy is significantly decreased.[34,42,43] Here, while the apparent activation energy decreases, the pre-exponential of the rate decreases with the electric field, suggesting an experimental correlation between the two or a change in the mechanism or geometry of the reaction site.

In addition, the correlation between the turnover frequency (TOF) and the metal particle size in the presence and absence of the electric field has also been investigated. They classify the TOF into those dependent on the surface area of the metal particles (TOF-s) and those dependent on the periphery of the metal particles (TOF-p), as described in eqn (1) and (2). In general catalytic reactions with heating, the TOF divided by the surface area (TOF-s) takes a constant value, while the TOF divided by the perimeter area (TOF-p) takes a constant value in reactions with the addition of an electric field.[34,40,43] The TOF (TOF-p) takes a constant value for reactions with an applied electric field.[34,40,43] This is evidence that the reaction with an applied electric field is active only around the supporting metal. Furthermore, only when an electric field was applied, a unique peak related to the Grotthuss mechanism was detected *in situ* infrared measurements, suggesting the appearance of proton hopping on the catalyst surface.[34,40,42,51] These findings suggest that the reaction under the applied
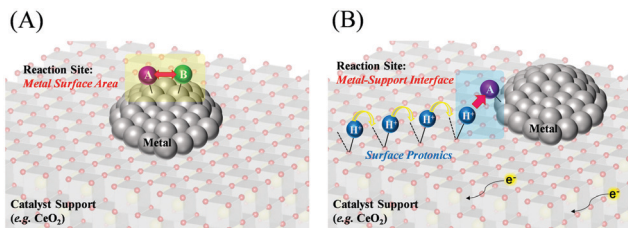
Fig. 3 Schematic reaction mechanisms; (A) without an applied electric field, (B) with an applied electric field.

electric field has a completely different reaction pathway from the conventional process, as generalized in Fig. 3, but on the other hand the ohmic Joule heating does indeed come from the transport of protons on the surface of the support, since this is the dominating conduction mechanism in the catalyst material. In the case of catalysis by heat without an applied electric field, the reaction takes place on the metal catalyst surface based on the Langmuir–Hinshelwood mechanism, whereas the catalysis with an applied electric field appears to proceed with the activated protons reacting with the reactants around the metal. The proton transfer can be assigned to proton conduction from dissociated water and hydrogen adsorbed on the catalyst support surface, resulting in a net flux of protons as a result of the current due to the DC electric field.

Equally interestingly, in the presence of an electric field, some reactions appear to proceed beyond thermodynamic equilibrium. This has been suggested to be due to the activation of irreversible reaction pathways.[18,19,34,35,37,38,49,52]

In the following, we discuss the contribution of surface protonics to various catalytic reactions: (1) ammonia synthesis,[39,41–44] (2) methane steam/dry reforming,[34] (3) water gas shift,[51] and (4) methylcyclohexane dehydrogenation.[37,38] Irreversible properties derived from the electric field will also be discussed.

$$\text{TOF-s} = \frac{\text{Reacted reactant mole rate } [\text{mol s}^{-1}]}{\text{Metal (surface area) mole } [\text{mol}]} \quad (1)$$

$$\text{TOF-p} = \frac{\text{Reacted reactant mole rate } [\text{mol s}^{-1}]}{\text{Metal (perimeter) mole } [\text{mol}]} \quad (2)$$

Detailed assessment of selected reactions

Here, we describe each reaction studied, discussing thermodynamics and catalysis, and the enhanced catalysis achieved by the electrical field.

Ammonia synthesis

More than 180 million tons of ammonia is produced annually on a very large industrial scale and is widely used as a raw material for chemical fertilizers, textiles, and refrigeration. The most established industrial route for ammonia synthesis is the Haber–Bosch process,[53–55] which uses iron-based catalysts for the exothermic reaction:

$$N_2(g) + 3H_2(g) \leftrightarrow 2NH_3(g) \quad \Delta H^0_{298} = -45.94 \text{ kJ mol}^{-1} \quad (3)$$
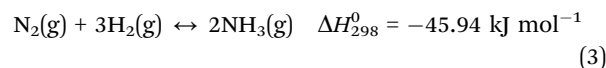
This process is an artificial nitrogen fixation process. The reaction mechanism over a heterogeneous catalyst is called the "dissociation mechanism".[56,57] Nitrogen dissociation is the rate-determining step in the Haber–Bosch process, which requires harsh reaction conditions of 20–40 MPa and 673–873 K due to its thermodynamic and kinetic limitations.[58]

Many possibilities to increase the efficiency of ammonia production have been extensively studied. The most popular catalyst for ammonia synthesis is based on iron-promoted complexes.[59] However, in 1972, Aika et al. reported that supported Ru is a more active catalyst that allows lower temperatures and hence also lower operating pressures.[60,61] The study of supported Ru catalysts allowed us to reduce the reaction temperature and pressure required for the Haber–Bosch process.[62–68]

Alternative ammonia synthesis routes including plasma,[69] photocatalysis,[70] and electrolysis[71] have been studied, showing the potential for low-temperature ammonia synthesis with better yields and efficiency.

Recently, Manabe et al. demonstrated a new catalytic ammonia synthesis process using an electric field and were the first to show surprisingly high ammonia synthesis rates at low temperatures.[42] Such a process has a higher energy efficiency than the plasma-based process. With electric field and current enhancement, a supported Ru/SrZrO₃ catalyst achieved an astonishing ammonia synthesis rate of more than 30 mmol g$_{cat}$$^{-1}$ h^{-1} and 0.9 MPa at a low temperature. Fig. 4(B) shows Arrhenius plots for ammonia synthesis at 0.1–0.9 MPa in the region 463–634 K with and without the electric field.

Application of an electric field at 0.9 MPa decreased the apparent activation energy from 121 kJ mol^{-1} to 37 kJ mol^{-1}.
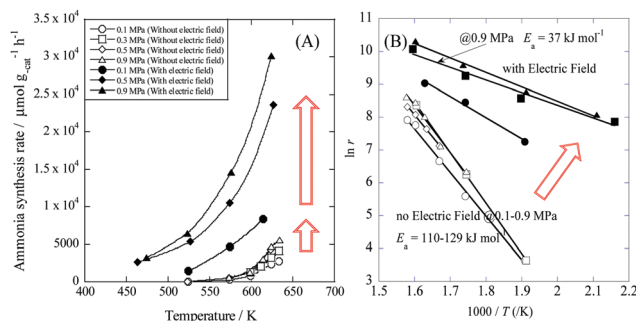

Fig. 4 Temperature and pressure dependence of ammonia synthesis rate with/without an electric field. (A) Temperature dependence of the ammonia synthesis rate at 0.1–0.9 MPa. (B) Arrhenius plots for each reaction: catalyst bed temperature, 463–634 K; catalyst, Cs/Ru/SrZrO₃, 200 mg; flow, N₂ : H₂ = 1 : 3, total 240 sccm; current, 0 or 6 mA. Reproduced with permission from literature.[42]

Furthermore, the partial pressure dependence of H_2 increased from -0.2 to 0, and that of N_2 decreased from 0.7 to 0.2. The difference in these trends is so large that the reaction mechanism is considered to be changed by the application of an electric field.[42]

Isotope exchange studies with isotopic nitrogen ($^{30}N_2$) confirmed that N_2 dissociation was significantly enhanced by the application of an electric field.[42] In addition, H/D isotope effect tests demonstrated that proton hopping on the catalyst surface plays an important role in catalyzing ammonia synthesis;[41] N_2 dissociation is thought to proceed through a milder pathway by using adsorbed protons in the electric field to hydrogenate N_2. Such a mechanism is called the "association mechanism".[39]

Density functional theory (DFT) calculations were used to investigate the effect of active metals on the rate of ammonia synthesis, both with and without an electric field.[44] Comparing several supported metals (Ru, Fe, Co, Ni, Pd, and Pt), the order was Ru > Fe > Co > Ni > Pd = Pt in the absence of the electric field, while a different trend was observed in the presence of electric field (Fe > Ni > Ru > Co > Pd > Pt). In addition, TOF-p and E_{N_2H} formation showed a linear correlation with the electric field (see Fig. 5). This is important evidence for a unique reaction pathway leading to the formation of N_2H intermediates.

A deviation from Arrhenius behavior in an intermediate-temperature region ($373\ K < T < 473\ K$) was observed over 1 wt% Ru/CeO_2 catalyst on the ammonia synthesis in the electric field (Fig. 6).[72] Two investigations of (i) P_{H_2} dependence on catalytic activity and (ii) the observation of surface OH group using *in situ* IR measurements revealed that the proton coverage over the catalyst surface is a critical factor for this non-Arrhenius behavior. In this temperature region, the proton coverage increases with lowering the temperature, and activated surface protonics leads to the higher ammonia synthesis rate. The appearance of surface protonics under NH_3 synthesis (*i.e.* dry atmosphere) has also been concluded from AC impedance measurements[73] on porous (R.D. = 60%) as compared to dense (R.D. = 90%) $SrZrO_3$ pellets: only the porous sample showed enhancement of conductivity at lower temperatures ($<723\ K$) when the gas atmosphere was switched from N_2 to
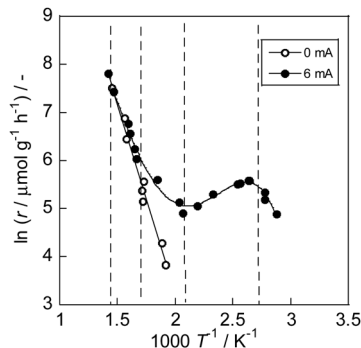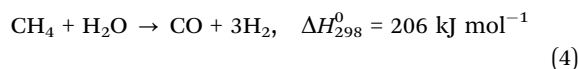

Fig. 6 Arrhenius plots for NH_3 synthesis rate (r) over 1 wt% Ru/CeO_2 with/without an electric field (0 or 6 mA) under $P_{H_2} = 0.75$ atm. Reproduced with permission from literature.[72]

$N_2 : H_2 = 1 : 3$. Furthermore, the porous sample exhibited a H/D isotope effect, contrary to the dense sample. These observations emphasize that the proton conduction takes place mainly on the grain surface, not in bulk, and that surface protons are dominant charge carriers under ammonia synthesis atmospheres. So far, the energy efficiency of this reaction in the electric field is $>1\ kW\ h\ kg^{-1}$-NH_3, and it is still rather high. We have to decrease it by the better catalyst design.

In the NH_3 synthesis using the electric field, the hydrogenation of N_2 proceeds by the "associative mechanism" that can proceed under milder conditions than the "dissociative mechanism"; this allows the reaction to proceed at temperatures as low as 473 K. In particular, the increase in surface proton coverage at lower temperatures contributes significantly to the improvement of catalytic activity.

Steam reforming and dry reforming of methane

The demand for hydrogen is increasing every year thanks to its wide range of use and high potential as a clean secondary energy source that can be easily converted into electricity by fuel cells with water as the only by-product. Most of the industrially produced hydrogen is formed by steam reforming (SR) with methane by the eqn (4).

$$CH_4 + H_2O \rightarrow CO + 3H_2, \quad \Delta H^0_{298} = 206\ kJ\ mol^{-1}$$

(4)

This reaction is usually carried out at high temperatures of at least 973 K using Ni catalysts because it is a very endothermic reaction, and methane has high structural stability.[74,75] Such harsh conditions are associated with several problems, such as catalyst deactivation and the need for complex processes with heat exchangers and highly thermostable structural materials. Therefore, a novel process which can work at lower temperatures is promising. It has been shown that the use of Pd-supported catalysts with a DC electric field promotes methane steam reforming, in what was referred to as an irreversible path and named electroreforming, ER.[34,35] By applying the electric field (EF) on the catalyst (Fig. 7(A)), high
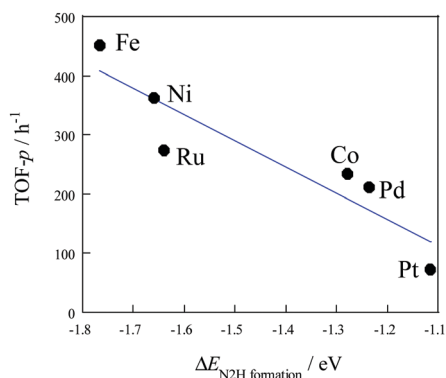

Fig. 5 TOF-p as a function of $\Delta E_{N2H\ formation}$ with an electric field, 0.1 MPa, 373 K, 6 mA. Reproduced with permission from literature.[44]
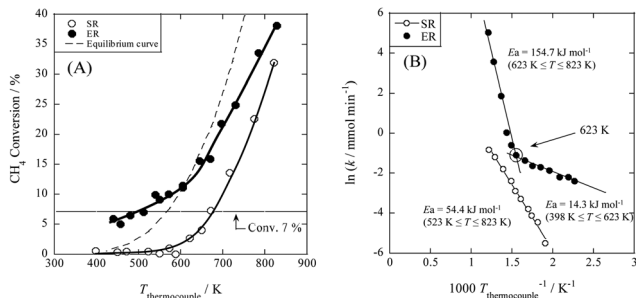
Fig. 7 Temperature dependencies of catalytic activity with or without electric field (EF). (A) Activities for catalytic steam reforming by heat (SR) and applying EF (ER); (B) Arrhenius plots for both reactions, preset temperature, 398–823 K; catalyst, 1.0 wt% Pd/CeO$_2$, 80 mg; flow, CH$_4$: H$_2$O : Ar : He = 12 : 24 : 12 : 72, total flow rate 120 sccm; current, 0 or 5 mA. Reproduced with permission from literature.[34]

catalytic activity was observed even at low temperatures such as 473 K, where otherwise no reaction occurs. From the partial pressure dependence, the reaction rate equations with/without the electric field can be described as follows (eqn (5) and (6)).

$$r = kP_{CH_4}^{0.9}P_{H_2O}^{0.1} \quad \text{(SR at 673 K)} \tag{5}$$

$$r = kP_{CH_4}^{0.25}P_{H_2O}^{0.79} \quad \text{(SR at 673 K)} \tag{6}$$

Thus, for the same methane conversion rate, SR and ER showed completely different partial pressure dependencies. When an electric field was applied, the methane partial pressure dependence decreased and the water pressure dependence increased, with the water partial pressure dependence exceeding the methane partial pressure dependence. As shown in Fig. 8(B), the Arrhenius plots of SR and ER show that the apparent activation energy of ER decreases significantly from 54.4 kJ mol^{-1} to 14.3 kJ mol^{-1} when the electric field is applied. These results indicate that ER proceeds through a different reaction pathway from that of SR, which has lower activation energy at temperatures below 623 K.

In order to elucidate the reaction mechanism with EF in more detail, we performed *operando* diffuse reflectance infrared Fourier transform spectroscopy (DRIFTS) measurements for both SR and ER. Fig. 8(A) shows the results of comparison under several conditions: the peak observed at 855 cm^{-1} is
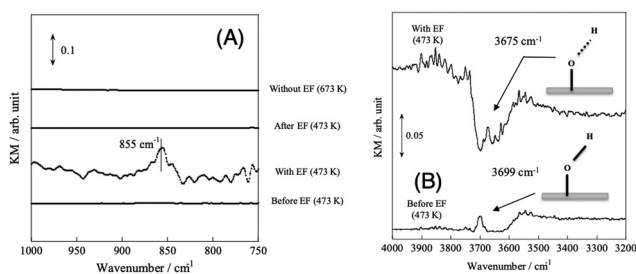
attributed to the rotation of adsorbed water,[76,77] indicating that proton hopping occurs *via* O–H groups and water molecules based on the Grotthuss mechanism. As shown in Fig. 8(B), when an electric field was applied, the peak of O–H bond shifted to a lower wavenumber due to the stretching of O–H bond length, indicating the weakening of the O–H bond. Furthermore, AC impedance measurements of porous CeO$_2$ pellets were performed to evaluate their electrical properties in terms of surface proton conduction.[78] As shown in Fig. 9, the temperature dependence was different between the dry (Ar) and wet (Ar + H$_2$O) conditions, and the conductivity enhancement in the low-temperature region was observed only in the wet condition. This phenomenon can be attributed to the increase of adsorbed water on the grain surface with decreasing temperature, which enhanced the surface proton conduction.[79–90] This result is in good agreement with the results of the *operando*-DRIFTS measurements. To further investigate the contribution of proton hopping, we evaluated the quantitative changes in gas-phase methane at 3016.6 cm^{-1}.[91] The infrared band intensity of gas-phase methane at 473 K was not identical in the presence or absence of H$_2$O, and the infrared band intensity decreased sharply while H$_2$O was supplied. These results suggest that H$_2$O is strongly involved in the activation of methane in the ER. In order to confirm whether methane is activated by proton collisions originating from the Grotthuss mechanism, kinetic isotope effects were evaluated using D$_2$O. As a result, the decrease in infrared intensity was larger when D$_2$O was used than when H$_2$O was used, suggesting that the reverse kinetic isotope effect (KIE) appears.[92–95] In addition, from the potential energy point of view, the energy levels with steep potential curves are formed in the triatomic transition state, and the discrepancy of the zero-point energy (ZPE) is enlarged.[35] Thus, the activation energy is lower when the isotope (D$_2$O) is used. These results indicate that the dissociative adsorption of methane at low temperatures is facilitated by the protonic nature of the surface, which promotes proton collisions with methane. The *operando*-DRIFTS study and AC impedance measurements revealed that the proton hopping on the catalyst surface is an essential factor for high methane conversion at low temperatures during ER.

Fig. 8 *Operando*-DRIFTS spectra with/without EF. (A) O–H rotating region, (B) O–H stretching region, catalyst, CeO$_2$ or 1.0 wt% Pd/CeO$_2$; flow, CH$_4$: H$_2$O : Ar = 1 : 2 : 62, total flow rate 65 sccm; current, 0 or 5 mA. Reproduced with permission from literature.[34]

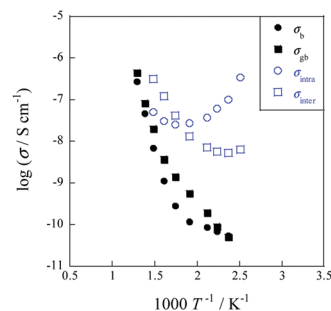**Fig. 9** Electrical conductivity of porous CeO$_2$ as a function of inverse temperature under dry and wet conditions (P_{H_2O} = 0.026 atm). Reproduced with permission from literature.[78]
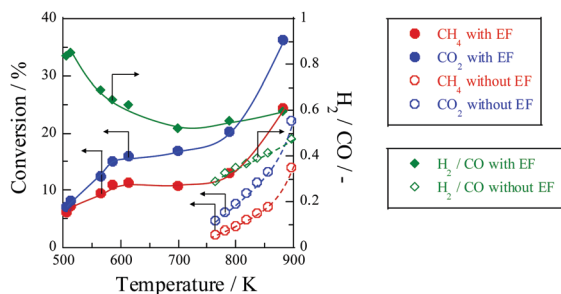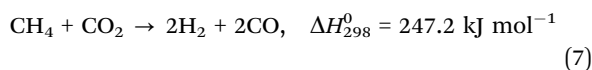
Fig. 10 Temperature dependence for catalytic activities with EF over 0.88 wt% Ni/10 mol% La–ZrO$_2$ catalyst, CH$_4$:CO$_2$:Ar = 1:1:2, total flow rate: 20–200 sccm; input current: 3 mA; catalyst weight: 100 mg; furnace temperature: 505–880 K (with EF) and 764–897 K (without EF). Reproduced with permission from literature.[40]

Dry reforming of methane (DRM) is recognized as another important hydrogen and/or syngas production processes, as shown in eqn (7).[96–100]

$$CH_4 + CO_2 \rightarrow 2H_2 + 2CO, \quad \Delta H^0_{298} = 247.2 \text{ kJ mol}^{-1}$$
$$(7)$$

Recently, DRM is attracting attention from the viewpoint of efficient utilization of natural gas and suppressing global warming.[101–104] Nevertheless, this reaction requires a high temperature, above 1073 K, because of its thermodynamic limitations, so some issues including expensive material for the reactor and coke deposition on the catalyst are known.[105,106] For resolving these problems and proceeding reaction efficiency even at low temperatures, a new DRM process that proceeds with less coke deposition has been strongly desired. Recently, Yabe et al. have achieved the promotion of DRM at low temperatures such as 473 K by imposing EF.[40,107] In their research, 1 wt% Ni/10 mol% La–ZrO$_2$ catalyst was used. Fig. 10 shows the temperature dependence of catalytic activity with/without the EF. Both CH$_4$ and CO$_2$ conversions are enhanced drastically at low temperatures by applying the EF, although the conventional catalytic reaction hardly proceeds. The apparent activation energy based on CH$_4$ and CO$_2$ consumption rates was evaluated at temperatures of 505–880 K with EF and 764–897 K without EF at similar conversion conditions. As shown in Table 1, the apparent activation energy was much lower by applying EF for each

Table 1 Apparent activation energy E_a, calculated from CH$_4$ and CO$_2$ consumption rate, for dry reforming of CH$_4$ with/without the EF over 0.88 wt% Ni/10 mol% La–ZrO$_2$ catalyst.[a] (Reproduced with permission from literature[40])

		E_a/kJ mol^{-1}	R^2 value/—
Without EF	CH$_4$	66.1	0.96
	CO$_2$	62.3	0.97
With EF	CH$_4$	8.2	0.99
	CO$_2$	12.1	0.99

[a] Reaction conditions: CH$_4$:CO$_2$:Ar = 1:1:2; 100 sccm total flow rate; 3.0 mA input current; 100 mg catalyst weight; 505–880 K (with EF) and 764–897 K (without EF) catalyst bed temperature.
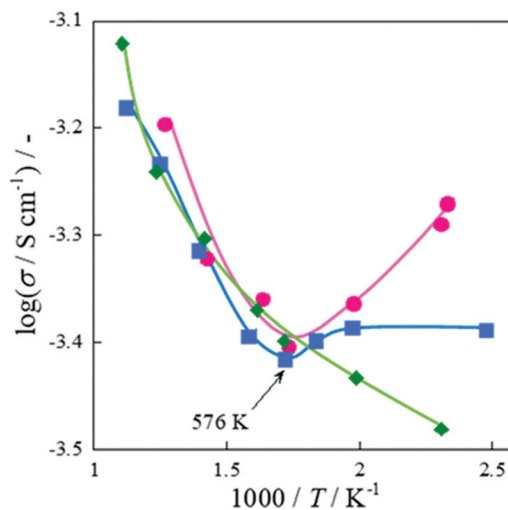

Fig. 11 Logarithmic apparent electrical conductivity as a function of inverse temperature with EF over 0.88 wt% Ni/10 mol% La–ZrO$_2$ catalyst, CH$_4$ (or CD$_4$):CO$_2$:Ar = 1:1:2 or CO$_2$:Ar = 1:3; total flow rate, 100 sccm; 3.0 mA input current; 100 mg catalyst weight; 404–856 K catalyst bed temperature. Reproduced with permission from literature.[40]

reactant, indicating that DRM with the EF proceeded via a totally different reaction path from the heated catalytic reaction. We have proposed that surface protonics on the catalyst surface induced by imposing EF promotes the catalytic reaction at low temperatures.[36] Assuming that the proton conduction on the catalyst surface contributes to high CH$_4$ and CO$_2$ conversion for DRM with EF, the apparent electrical conductivity behavior was assessed as shown in Fig. 11. The conductivity was calculated using eqn (8), where L denotes the catalyst bed height, S represents the area of electrodes, I shows the applied current and V stands for the response voltage.

$$\sigma = \frac{L}{S} \cdot \frac{I}{V} \quad (8)$$

As shown in Fig. 11, conductivity increased with decreasing temperature below 573 K in the CH$_4$ + CO$_2$ reaction, while conductivity decreased in the same temperature range in the CO$_2$ + Ar reaction. This behavior is close to that of the water-supplying state (under the wet condition), and the enhanced conductivity at low temperatures is interpreted as an increase in the amount of surface adsorbed species such as H$_2$O and hydroxyl groups with decreasing temperatures.[108–110] In this case, it is inferred that the surface proton species were formed by CH$_4$ and surface hydroxyl groups on La–ZrO$_2$ via the reverse water–gas shift reaction (RWGS: H$_2$ + CO$_2$ → CO + H$_2$O).

In the case of the CD$_4$ + CO$_2$ reaction, the conductivity in the low-temperature region was lower than that of the CH$_4$ + CO$_2$ reaction because the D species, such as D$_2$O and OD groups derived from CD$_4$, are heavier than the H species. Furthermore, we investigated the KIE of DRM with EF using CH$_4$/CD$_4$ and CO$_2$ (Fig. 12). In this experiment, pre-reduction with H$_2$ or D$_2$ was performed to produce H or D species, r_H and r_D were calculated as the CO production rate, and the value of r_D/r_H was evaluated. As a result, CO from CH$_4$ was calculated to be
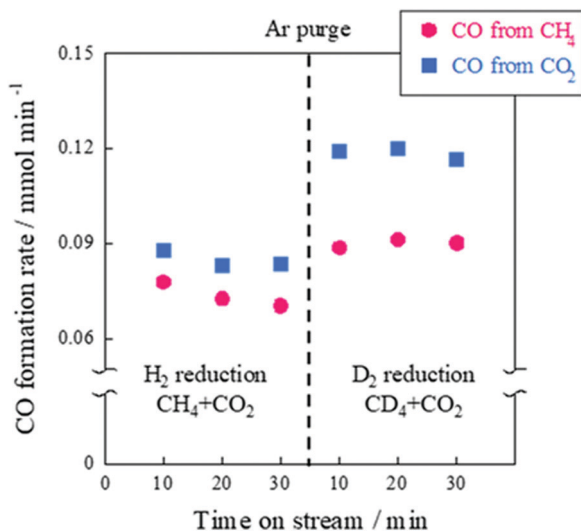
Fig. 12 CO formation rate with the EF over 0.88 wt% Ni/10 mol% La–ZrO$_2$ catalyst, CH$_4$ (or CD$_4$) : CO$_2$: Ar = 1 : 1 : 2; total flow rate, 100 sccm; 3.0 mA input current; 100 mg catalyst weight; 423 K furnace temperature. Reproduced with permission from literature.[40]

1.23 ± 0.08 and CO from CO$_2$ was calculated to be 1.39 ± 0.03. These results indicate an ''inverse'' KIE for the dissociation of both CH$_4$ and CO$_2$.[92,111–116] Furthermore, *operando*-DRIFTS measurements were performed to observe the surface adsorbed species of DRM in the presence of an electric field. According to the overall (Fig. 13(A)) and magnified (Fig. 13(B)) spectra, a specific peak corresponding to the rotation of adsorbed water at 850 cm^{-1} at 573 K was observed in the difference spectrum between the EF-applied and post-applied spectra, *i.e.*, only in the EF-applied spectrum. This water rotation is based on the Grotthuss mechanism, and this result is evidence of the appearance of surface proton conduction.

On the steam and dry reforming of methane, the energy efficiency is rather high compared to the exothermic reaction (*i.e.* ammonia synthesis, *etc.*). So far, about ∼70% of the electric power consumption has been used for the endothermic reaction, and it depends on the catalyst structure. Further improvement on the reaction energy efficiency is anticipated.
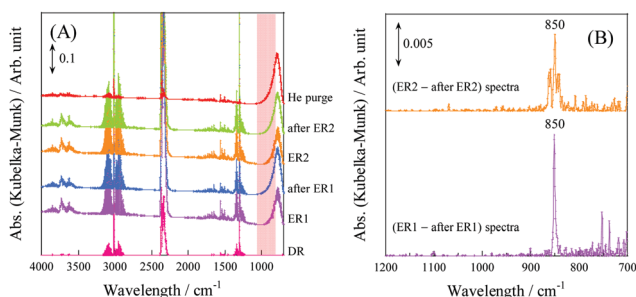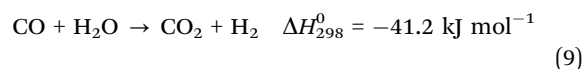

Fig. 13 *Operando*-DRIFTS spectra with/without EF. (A) Comparison of before/with/after applying EF (without EF, DR; with EF, ER). (B) Differential spectra with/after applying EF in H$_2$O rotation: 0.88 wt% Ni/10 mol% La–ZrO$_2$ catalyst; CH$_4$: CO$_2$: He = 3 : 3 : 34; 40 Sccm total flow rate; 9 mA current; 573 K preset temperature. Reproduced with permission from literature.[40]

By thorough investigations on steam reforming and dry reforming of methane, it was revealed that surface protonics efficiently promotes these reactions at low temperatures by the application of EF, which was evidenced by studies of *operando*-DRIFTS measurement, ''inverse'' KIE, and the electrical property of catalyst support.

Water gas shift reaction

The water gas shift (WGS) reaction is important for industrial hydrogen production. This reaction enables purifying produced hydrogen by steam reforming and adjusting the synthesis gas composition. Carbon monoxide (CO), which is produced as a byproduct in steam reforming, poisons electrodes in polymer electrolyte membrane fuel cells (PEMFCs).[117–119] The WGS reaction is exothermic as presented in eqn (9).

$$CO + H_2O \rightarrow CO_2 + H_2 \quad \Delta H^0_{298} = -41.2 \text{ kJ mol}^{-1}$$

(9)

Thus, it is thermodynamically favorable at low temperatures, but kinetically limited. Accordingly, the WGS reaction is well suited for catalytic promotion at lower temperatures.

An effective solution to these problems is to apply an electric field to the heterogeneous catalyst.[51] When a DC electric field was applied (3 mA, 2.9 W) to a Pt/La–ZrO$_2$ catalyst, the CO conversion increased from 0% to 47.1% even at 423 K.[1] To investigate the difference in the reaction rate with and without the electric field, we compared the apparent activation energy. As a result, the apparent activation energy was reduced to almost half when the electric field was applied (98.3 kJ mol^{-1} without EF, 50.9 kJ mol^{-1} with EF). In order to compare the behavior with and without the applied electric field, the partial pressure dependence of each reactant (CO, H$_2$O) on the rate was investigated. The results showed that when the electric field was applied at 553 K, the reaction partial pressure of CO changed from −0.28 to 0.33 and that of H$_2$O from 0.49 to 0.57. In the case of WGS with the electric field, the CO partial pressure dependence changed from negative to positive and CO adsorption was suppressed; the change in the H$_2$O partial pressure dependence was assumed to originate from the surface ionic conductivity based on the Grotthuss mechanism. By this mechanism, protons move through the rotating surface adsorbed water with a weak electric current, thus accelerating the surface catalytic reaction. The changes in the partial pressure dependence of each reactant indicate that the electric field accelerates the reaction at low temperatures. These changes suggest that the WGS reaction using an electric field proceeds through a different pathway than the conventional reaction. In order to clarify this reaction pathway, we evaluated the H/D isotope effect. As shown in Table 2, the primary isotope effect was confirmed, with r_D/r_H having the same value of 0.317 in the presence and absence of EF. This result indicates that H$_2$O is activated on the catalyst support, but not on the overloaded Pt, and that O–H dissociation is not part of the rate-determining step for both reactions. Next, we performed a

Table 2 H/D isotope effect for WGS (reproduced with permission from literature[51])

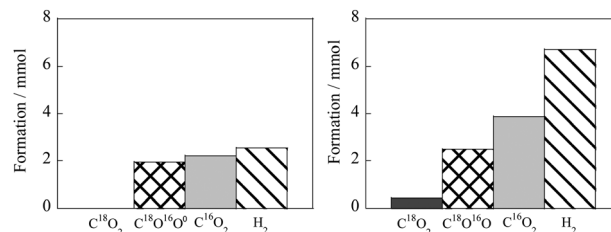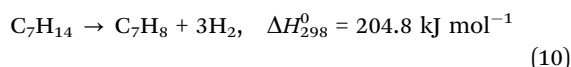|	r_D/mmol min^{-1}	r_H/mmol min^{-1}	r_D/r_H/—
Without EF	0.004	0.013	0.317
With EF	0.025	0.078	0.317

transient experiment in which the reactants (CO and H_2O) were periodically introduced. The transient production of CO and H_2 was monitored using a quadrupole mass spectrometer (Q-Mass). It is clear from the results summarized in Table 3 that in the reaction without EF, the amount of CO_2 and H_2 produced was almost the same at the fourth introduction of CO, which was stoichiometric. On the other hand, in the reaction with EF, the amount of CO_2 produced exceeded that of H_2 in all cycles. This suggests that a redox mechanism using surface-lattice oxygen and H_2O occurred during the EF reaction. Based on this, we investigated the transient production of CO_2 using the ^{18}O isotope. As shown in Fig. 14, $C^{18}O_2$ was not observed at all in the reaction without EF, while $C^{18}O_2$ and $C^{18}O^{16}O$ were detected in abundance in the reaction with EF. These results indicate that the lattice oxygen plays an important role and that the reaction mechanism in the EF reaction is the Mars–van Krevelen mechanism. These investigations indicate that it is possible to promote the WGS reaction at low temperatures by surface reactions based on the Mars–van Krevelen mechanism by applying an electric field.

Methylcyclohexane dehydrogenation

The methylcyclohexane (MCH)–toluene–hydrogen cycle is promising and interesting as a liquid organic hydrogen carrier system. Dehydrogenation of MCH, eqn (10), is an endothermic reaction. It typically requires temperatures above 623 K due to its kinetic limitations, even over Pt catalysts.[120]

Table 3 Transient responses during cyclic introductions of CO and H_2O over Pt/La–ZrO$_2$ with/without EF, at 553 K for with EF and at 723 K for without EF (reproduced with permission from literature[51])

		With EF at 553 K		Without EF at 723 K	
		CO_2 formation/ mmol	H_2 formation/ mmol	CO_2 formation/ mmol	H_2 formation/ mmol
1st	CO introduction	24.65	7.42	12.17	1.77
	H_2O introduction	0.00	8.24	0.00	2.16
2nd	CO introduction	12.13	6.52	2.64	1.91
	H_2O introduction	0.00	6.59	0.00	3.41
3rd	CO introduction	14.99	9.96	3.04	2.87
	H_2O introduction	0.00	0.00	0.00	0.00
4th	CO introduction	7.13	3.29	2.40	2.22

Fig. 14 Transient formation amounts of isotopic CO_2 during transient tests using ^{18}O, left: without EF, right: with EF. Reproduced with permission from literature.[51]

$$C_7H_{14} \rightarrow C_7H_8 + 3H_2, \quad \Delta H^0_{298} = 204.8 \text{ kJ mol}^{-1}$$

(10)

If this dehydrogenation temperature could be lowered efficiently, a clean energy society e.g. reducing energy consumption or using low-grade heat can be realized.[120–123] Nevertheless, this reaction is strictly limited by the thermodynamic equilibrium, particularly at low temperatures. To exceed this equilibrium limitation and promote the dehydrogenation at low temperatures irreversibly, we have investigated irreversible MCH dehydrogenation with a DC electric field over supported Pt catalysts.[37,38,49] Results presented in Table 4 show that the catalytic activity was enhanced markedly by the DC electric field at low temperatures.

Notably, at 423 K, the catalytic activity showed 21.6% hydrogen yield, which exceeds the thermodynamic equilibrium hydrogen yield of 5.5% at this temperature. From the Arrhenius plots (Fig. 15), the apparent activation energies with and without electric field were 28.6 and 55.6 kJ mol^{-1}, respectively. These results indicate that the applied electric field promotes the MCH dehydrogenation, and that the reaction mechanism involved must be different from the one in operation without the electric field.

To investigate the reaction mechanism, partial pressure dependencies of MCH, toluene and hydrogen were assessed and are shown in Table 5, allowing the MCH dehydrogenation reaction rate to be expressed by eqn (11)

$$r_{\text{dehydrogenation}} = k[\text{MCH}]^a[\text{Toluene}]^b[\text{H}_2]^c \quad (11)$$

Generally, gaseous hydrogen promotes the hydrogenation of toluene, which is the reverse reaction in this case. In the absence of the electric field, there was a negative dependence on the hydrogen partial pressure ($c < 0$) in eqn (11). On the other hand, when an electric field was applied, the reaction rate showed an unusual positive dependence on the hydrogen partial pressure. It has been reported that the positive dependence of the hydrogen partial pressure indicates the acceleration of the reaction by proton hopping at the catalyst surface.[34,36] Therefore, proton species may be an important factor in accelerating the MCH dehydrogenation reaction in an electric field.

Furthermore, the isotope effect was investigated by supplying MCHD (i.e., C_7D_{14}) and D_2 during the reaction with and without an electric field, as shown in Table 6. The isotope

Table 4 Temperature dependences of catalytic activity in a kinetic condition on 3 wt% Pt/CeO$_2$ with and without the electric field; gas supply: MCH : Ar = 6.4 : 30 (total flow rate 36.4 mL min^{-1}), EF: constant current of 3 mA.[a] (Reproduced with permission from literature[37])

Reaction temperature/K	Equilibrium limitation/%	With EF			Without EF		
		T_{tc}/K	H$_2$ yield/%	CH$_4$ production/10^{-2} μmol min^{-1}	T_{tc}/K	H$_2$ yield/%	CH$_4$ production/10^{-2} μmol min^{-1}
423	5.5	442	21.6	1.1	422	0.8	n.d.
473	25.2	479	30.2	2.4	468	5.6	n.d.
523	72.0	522	51.8	4.1	523	21.5	1.6
573	98.7	572	88.3	14.0	566	52.5	5.2

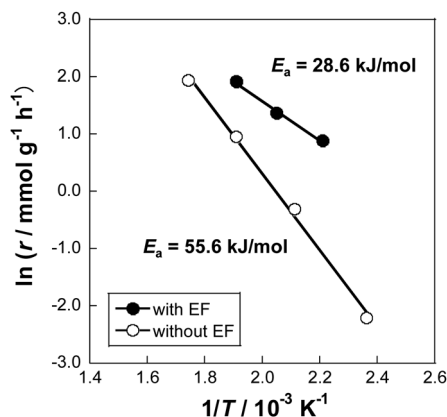[a] T_{tc}: catalyst bed temperature measured using a thermocouple.

Fig. 15 Arrhenius plots for 3 wt% Pt/CeO$_2$ catalyst with and without the electric field (EF): gas supply, MCH : Ar = 6.4 : 30 (total flow rate 36.4 mL min^{-1}); EF: constant current of 3 mA. Reproduced with permission from literature.[37]

Table 5 Dependence of partial pressure and reaction rate for (a) methyl-cyclohexane, (b) toluene, and (c) hydrogen over 3 wt% Pt/CeO$_2$ in methylcyclohexane dehydrogenation with the electric field at 423 K and without electric field at 523 K; EF: constant current 3 mA; gas supply: C$_7$H$_{14}$: Ar = (3.2, 6.4, 9.6, 11.3) : (53.2, 50.0, 46.8, 45.1), C$_7$H$_{14}$: C$_7$H$_8$: Ar = 6.4 : (1.0, 2.0, 3.0, 4.0) : (49.0, 48.0, 47.0, 46.0) and C$_7$H$_{14}$: H$_2$: Ar = 6.4 : (4.0, 7.0, 9.0, 12.0) : (46.0, 43.0, 41.0, 38.0). (Reproduced with permission from literature[37])

Condition	a (MCH)	b (toluene)	c (H$_2$)
With EF (423 K)	0.35	−0.07	0.15
Without EF (523 K)	0.49	−0.18	−0.13

effects were evaluated using the isotope ratio of the rate constants, k_D/k_H. This value is typically less than 1 due to the higher stability of the chemical bonds of the heavier isotopes (low zero-point energy (ZPE)).[35] The results for no electric field are consistent with those for MCHD, which are 0.67 for MCH$_D$/H$_2$ and 0.69 for MCH$_D$/D$_2$. The results confirmed the kinetic isotope effect (KIE) in the case without the electric field. However, it was found that the k_D/k_H value increased with increasing deuterium supply when an electric field was applied. This inverse KIE was observed due to the extended ZPE discrepancy between the isotopes in the physisorbed to three-atom transition state when the C–H–H configuration was formed by

Table 6 MCH dehydrogenation using isotope; 3 wt% Pt/CeO$_2$ catalyst; gas supply: MCH : H$_2$ (or D$_2$) : Ar = 6.4 : 4 : 46 (total flow 56.4 mL min^{-1}); EF: constant current of 3 mA. (Reproduced with permission from literature[37])

Condition		T_{tc}[a]/ K	H$_2$ production rate/μmol min^{-1}	H$_2$ yield/ %	k_D/ k_H/—
With EF (423 K)	MCH$_H$/H$_2$	445	148	18.8	—
	MCH$_H$/D$_2$	441	178	22.6	1.20
	MCH$_D$/H$_2$	445	180	22.9	1.22
	MCH$_D$/D$_2$	442	209	26.6	1.42
Without EF (523 K)	MCH$_H$/H$_2$	519	247	31.5	—
	MCH$_H$/D$_2$	519	255	32.5	1.03
	MCH$_D$/H$_2$	518	165	21.0	0.67
	MCH$_D$/D$_2$	520	170	21.7	0.69

[a] T_{tc}: catalyst bed temperature measured using a thermocouple.

proton collisions.[35,92,94,95,124] Thus, the inverse KIE indicates that proton collisions promote MCH dehydrogenation in the electric field. It has also been suggested that when MCH dehydrogenation passes through the three-atom transition due to proton hopping, it has an inhibitory effect on the reverse reaction, toluene hydrogenation, because hydrogenation in an electric field requires large apparent activation energy.[37] As discussed in this section, surface protonation by the application of an electric field can achieve irreversible MCH dehydrogenation and highly efficient hydrogen production even at temperatures as low as 423 K. The electrical energy demand for this reaction in the electric field is rather small, and about 70% of energy efficiency based on the electric power consumption and the reaction enthalpy has been achieved.

Discussion

As described in "Detailed Evaluation of Selected Reactions," we have thoroughly elucidated the significance of the effects of electric field on the catalytic activity. As a result, we discovered a novel catalytic reaction mechanism that proceeds in a low-temperature electric field, different from conventional (heated) catalytic reactions.[1,2] The enhancement seems not to stem from ohmic Joule heating, based on temperature measurements with thermocouples near and in the catalyst and by the Debye–Waller factor in EXAFS. The frequency factor was small because the apparent activation energy was greatly reduced by the

application of the electric field, and the reaction mechanism changed from a reaction on the metal surface to a reaction at the interface of the metal and the substrate. There are three important phenomena: (i) *in situ* DRIFTS measurements to evaluate the behavior of surface adsorbents showed proton hopping on the catalyst support surface based on the Grotthuss mechanism.[34,35] (ii) Considering the "inverse" KIE theory, protons with kinetic energy collide with stable reactants and accelerate the rate-determining step of the reaction.[34,37,38] (iii) EIS measurements revealed that surface ionic conduction occurs on the catalyst support at lower temperatures.[34,36] These three are strong evidence to support a significant increase in the reaction rate of the catalytic process by the application of this electric field. In order to further explain the apparent irreversibility, further studies from the perspective of "dynamics" such as *ab initio* molecular dynamics (AIMD) simulations are desirable. One example is the quantitative evaluation of the collision frequency of protons. This allows us to know how much kinetic energy is consumed to form an intermediate in the transition state. It is also important to find new catalytic materials that can improve the efficiency and performance of this process. We propose "topological ionic conductors" as a unique candidate for this purpose. As their physicochemical properties, we expect partial activation of ion conduction (surface proton conduction) and reduction of Joule heat loss. In order to create such a material, we need to evaluate in parallel (a) the bulk conductivity by DC conduction measurements and (b) the surface ionic conductivity by AC impedance measurements. If this can be achieved, the process will allow for much higher catalytic activity and also control the selectivity to the desired product. If this happens, highly efficient processes for small-scale, on-site, and on-demand production could be established in the future.

Conclusion

A method of applying an electric field to semiconductor catalysts was proposed as a way to make catalytic reactions low temperature and on-demand. The working theory of the method is summarized and its application is described. For further development, it is suggested to develop new materials and structures that can promote surface protonics, and simpler evaluation methods for them. Further research in this area is highly anticipated.

Conflicts of interest

There are no conflicts to declare.

Acknowledgements

Notes and references

1 S. Ogo and Y. Sekine, *Chem. Rec.*, 2017, **17**(8), 726–738.
2 M. Torimoto, K. Murakami and Y. Sekine, *Bull. Chem. Soc. Jpn.*, 2019, **92**(10), 1785–1792.
3 F. Shen, K. Li, D. Xu, R. Yan, T. Chen, R. Zhan and H. Lin, *Mol. Catal.*, 2019, **476**, 110536.
4 K. Li, K. Liu, H. Ni, B. Guan, R. Zhan, Z. Huang and H. Lin, *Mol. Catal.*, 2018, **459**, 78–88.
5 K. Liu, K. Li, D. Xu, H. Lin, B. Guan, T. Chen and Z. Huang, *J. Shanghai Jiaotong Univ.*, 2018, **23**(1), 8–17.
6 K. Li, K. Liu, D. Xu, H. Ni, F. Shen, T. Chen, B. Guan, R. Zhan, Z. Huang and H. Lin, *Chem. Eng. J.*, 2019, **369**, 660–671.
7 K. Li, D. Xu, K. Liu, H. Ni, F. Shen, T. Chen, B. Guan, R. Zhan, Z. Huang and H. Lin, *J. Phys. Chem. C*, 2019, **123**(16), 10377–10388.
8 F. Che, J. T. Gray, S. Ha, N. Kruse, S. L. Scott and J.-S. McEwen, *ACS Catal.*, 2018, **8**(6), 5153–5174.
9 F. Che, J. T. Gray, S. Ha and J.-S. McEwen, *ACS Catal.*, 2017, **7**(10), 6957–6968.
10 F. Che, J. T. Gray, S. Ha and J.-S. McEwen, *ACS Catal.*, 2017, **7**(1), 551–562.
11 F. Che, S. Ha and J. McEwen, *Angew. Chem., Int. Ed.*, 2017, **56**, 3557–3561.
12 F. Che, S. Ha and J.-S. McEwen, *Appl. Catal., B*, 2016, **195**, 77–89.
13 F. Che, J. T. Gray, S. Ha and J.-S. McEwen, *J. Catal.*, 2015, **332**, 187–200.
14 V.-J. Lee, *Science*, 1966, **152**(3721), 514.
15 J.-S. McEwen, A. G. C. Ros, P. Gaspard, T. V. de Bocarmé and N. Kruse, *Catal. Today*, 2010, **154**(1–2), 75–84.
16 C. Périllat-Merceroz, G. Gauthier, P. Roussel, M. Huvé, P. Gélin and R.-N. Vannier, *Chem. Mater.*, 2011, **23**(6), 1539–1550.
17 D. Bhattacharyya and R. Rengaswamy, *Ind. Eng. Chem. Res.*, 2009, **48**(13), 6068–6086.
18 Y. Sekine, M. Haraguchi, M. Matsukata and E. Kikuchi, *Catal. Today*, 2011, **171**(1), 116–125.
19 K. Oshima, T. Shinagawa, M. Haraguchi and Y. Sekine, *Int. J. Hydrogen Energy*, 2013, **38**(7), 3003–3011.
20 Y. Sekine, M. Haraguchi, M. Tomioka, M. Matsukata and E. Kikuchi, *J. Phys. Chem. A*, 2010, **114**(11), 3824–3833.
21 C. G. Vayenas, S. Bebelis and S. Neophytides, *J. Phys. Chem.*, 1988, **92**(18), 5083–5085.
22 A. de Lucas-Consuegra, A. Princivalle, A. Caravaca, F. Dorado, C. Guizard, J. L. Valverde and P. Vernoux, *Appl. Catal., B*, 2010, **94**(3–4), 281–287.
23 A. Caravaca, A. de Lucas-Consuegra, C. Molina-Mora, J. L. Valverde and F. Dorado, *Appl. Catal., B*, 2011, **106**(1–2), 54–62.
24 I. V. Yentekakis, Y. Jiang, S. Neophytides, S. Bebelis and C. G. Vayenas, *Ionics*, 1995, **1**(5–6), 491–498.
25 M. Stoukides and C. G. Vayenas, *J. Catal.*, 1981, **70**(1), 137–146.
26 S. Kado, K. Urasaki, Y. Sekine and K. Fujimoto, *Chem. Commun.*, 2001, (5), 415–416.
27 M. Kraus, B. Eliasson, U. Kogelschatz and A. Wokaun, *Phys. Chem. Chem. Phys.*, 2001, **3**(3), 294–300.
28 T. Jiang, Y. Li, C. J. Liu, G. H. Xu, B. Eliasson and B. Z. Xue, *Catal. Today*, 2002, **72**(3–4), 229–235.
29 S. Kado, Y. Sekine, T. Nozaki and K. Okazaki, *Catal. Today*, 2004, **89**(1–2), 47–55.
30 Y. Sekine, K. Urasaki, S. Asai, M. Matsukata, E. Kikuchi and S. Kado, *Chem. Commun.*, 2005, (1), 78–79.
31 C. J. Liu, A. Marafee, B. Hill, G. H. Xu, R. Mallinson and L. Lobban, *Ind. Eng. Chem. Res.*, 1996, **35**(10), 3295–3301.
32 C. J. Liu, A. Marafee, R. Mallinson and L. Lobban, *Appl. Catal., A*, 1997, **164**(1–2), 21–33.
33 A. Marafee, C. J. Liu, G. H. Xu, R. Mallinson and L. Lobban, *Ind. Eng. Chem. Res.*, 1997, **36**(3), 632–637.
34 R. Manabe, S. Okada, R. Inagaki, K. Oshima, S. Ogo and Y. Sekine, *Sci. Rep.*, 2016, **6**, 38007.
35 S. Okada, R. Manabe, R. Inagaki, S. Ogo and Y. Sekine, *Catal. Today*, 2018, **307**, 272–276.
36 R. Inagaki, R. Manabe, Y. Hisai, Y. Kamite, T. Yabe, S. Ogo and Y. Sekine, *Int. J. Hydrogen Energy*, 2018, **43**(31), 14310–14318.
37 K. Takise, A. Sato, K. Murakami, S. Ogo, J. G. Seo, K. Imagawa, S. Kado and Y. Sekine, *RSC Adv.*, 2019, **9**(11), 5918–5924.

38 K. Takise, A. Sato, S. Ogo, J. G. Seo, K.-I. Imagawa, S. Kado and Y. Sekine, *RSC Adv.*, 2019, **9**(48), 27743–27748.

39 K. Murakami, Y. Tanaka, S. Hayashi, R. Sakai, Y. Hisai, Y. Mizutani, A. Ishikawa, T. Higo, S. Ogo, J. G. Seo, H. Tsuneki, H. Nakai and Y. Sekine, *J. Chem. Phys.*, 2019, **151**(6), 064708.

40 T. Yabe, K. Yamada, K. Murakami, K. Toko, K. Ito, T. Higo, S. Ogo and Y. Sekine, *ACS Sustainable Chem. Eng.*, 2019, **7**(6), 5690–5697.

41 K. Murakami, R. Manabe, H. Nakatsubo, T. Yabe, S. Ogo and Y. Sekine, *Catal. Today*, 2018, **303**, 271–275.

42 R. Manabe, H. Nakatsubo, A. Gondo, K. Murakami, S. Ogo, H. Tsuneki, M. Ikeda, A. Ishikawa, H. Nakai and Y. Sekine, *Chem. Sci.*, 2017, **8**(8), 5434–5439.

43 A. Gondo, R. Manabe, R. Sakai, K. Murakami, T. Yabe, S. Ogo, M. Ikeda, H. Tsuneki and Y. Sekine, *Catal. Lett.*, 2018, **148**(7), 1929–1938.

44 K. Murakami, Y. Tanaka, R. Sakai, K. Toko, K. Ito, A. Ishikawa, T. Higo, T. Yabe, S. Ogo, M. Ikeda, H. Tsuneki, H. Nakai and Y. Sekine, *Catal. Today*, 2020, **351**, 119–124.

45 R. Sakai, K. Murakami, Y. Mizutani, Y. Tanaka, S. Hayashi, A. Ishikawa, T. Higo, S. Ogo, H. Tsuneki, H. Nakai and Y. Sekine, *ACS Omega*, 2020, **5**(12), 6846–6851.

46 A. D. Frantzis, S. Bebelis and C. G. Vayenas, *Solid State Ionics*, 2000, **136**, 863–872.

47 Y. Sekine, K. Urasaki, S. Kado, M. Matsukata and E. Kikuchi, *Energy Fuels*, 2004, **18**(2), 455–459.

48 K. Takise, A. Sato, K. Muraguchi, S. Ogo and Y. Sekine, *Appl. Catal., A*, 2019, **573**, 56–63.

49 M. Kosaka, T. Higo, S. Ogo, J. G. Seo, S. Kado, K. Imagawa and Y. Sekine, *Int. J. Hydrogen Energy*, 2020, **45**(1), 738–743.

50 T. Ano, S. Tsubaki, A. Liu, M. Matsuhisa, S. Fujii, K. Motokura, W.-J. Chun and Y. Wada, *Commun. Chem.*, 2020, **3**, 86.

51 Y. Sekine, K. Yamagishi, Y. Nogami, R. Manabe, K. Oshima and S. Ogo, *Catal. Lett.*, 2016, **146**(8), 1423–1428.

52 T. Yabe, K. Mitarai, K. Oshima, S. Ogo and Y. Sekine, *Fuel Process. Technol.*, 2017, **158**, 96–103.

53 J. S. Anderson, J. Rittle and J. C. Peters, *Nature*, 2013, **501**(7465), 84–87.

54 A. Mittasch, *Adv. Catal.*, 1950, **2**, 81–104.

55 G. Ertl, D. Prigge, R. Schloegl and M. Weiss, *J. Catal.*, 1983, **79**, 359–377.

56 K. Honkala, A. Hellman, I. N. Remediakis, A. Logadottir, A. Carlsson, S. Dahl, C. H. Christensen and J. K. Nørskov, *Science*, 2005, **307**, 555–558.

57 J. R. Jennings, *Catalytic ammonia synthesis, fundamentals and practice*, Springer, US, 1991, pp. 109–131.

58 P. Stoltze and J. K. Norskov, *Phys. Rev. Lett.*, 1985, **55**(22), 2502–2505.

59 B. Wilk, R. Pelka and W. Arabczyk, *J. Phys. Chem. C*, 2017, **121**(15), 8548–8556.

60 K. Aika, A. Ozaki and H. Hori, *J. Catal.*, 1972, **27**(3), 424–431.

61 K. Aika, A. Ohya, A. Ozaki, Y. Inoue and I. Yasumori, *J. Catal.*, 1985, **92**(2), 305–311.

62 Y. Ogura, K. Sato, S. Miyahara, Y. Kawano, T. Toriyama, T. Yamamoto, S. Matsumura, S. Hosokawa and K. Nagaoka, *Chem. Sci.*, 2018, **9**(8), 2230–2237.

63 M. Kitano, Y. Inoue, H. Ishikawa, K. Yamagata, T. Nakao, T. Tada, S. Matsuishi, T. Yokoyama, M. Hara and H. Hosono, *Chem. Sci.*, 2016, **7**(7), 4036–4043.

64 M. Kitano, Y. Inoue, Y. Yamazaki, F. Hayashi, S. Kanbara, S. Matsuishi, T. Yokoyama, S.-W. Kim, M. Hara and H. Hosono, *Nat. Chem.*, 2012, **4**(11), 934.

65 Y. Lu, J. Li, T. Tada, Y. Toda, S. Ueda, T. Yokoyama, M. Kitano and H. Hosono, *J. Am. Chem. Soc.*, 2016, **138**(12), 3970–3973.

66 J. Wu, Y. Gong, T. Inoshita, D. C. Fredrickson, J. Wang, Y. Lu, M. Kitano and H. Hosono, *Adv. Mater.*, 2017, **29**(36), 1700924.

67 M. Kitano, Y. Inoue, M. Sasase, K. Kishida, Y. Kobayashi, K. Nishiyama, T. Tada, S. Kawamura, T. Yokoyama and M. Hara, *Angew. Chem., Int. Ed.*, 2018, **57**(10), 2648–2652.

68 Y. Inoue, M. Kitano, K. Kishida, H. Abe, Y. Niwa, M. Sasase, Y. Fujita, H. Ishikawa, T. Yokoyama and M. Hara, *ACS Catal.*, 2016, **6**(11), 7577–7584.

69 R. Hawtof, S. Ghosh, E. Guarr, C. Y. Xu, R. M. Sankaran and J. N. Renner, *Sci. Adv.*, 2019, **5**(1), eaat5778.

70 J. John, D. K. Lee and U. Sim, *Nano Convergence*, 2019, **6**, 15.

71 T. Murakami, T. Nohira, T. Goto, Y. H. Ogata and Y. Ito, *Electrochim. Acta*, 2005, **50**(27), 5423–5426.

72 K. Murakami, Y. Tanaka, R. Sakai, Y. Hisai, S. Hayashi, Y. Mizutani, T. Higo, S. Ogo, J. G. Seo, H. Tsuneki and Y. Sekine, *Chem. Commun.*, 2020, **56**, 3365–3368.

73 Y. Hisai, K. Murakami, Y. Kamite, Q. Ma, E. Vøllestad, R. Manabe, T. Matsuda, S. Ogo, T. Norby and Y. Sekine, *Chem. Commun.*, 2020, **56**, 2699–2702.

74 J. R. Rostrup-Nielsen, *J. Catal.*, 1973, **31**(2), 173–199.

75 C. Bernardo, I. Alstrup and J. Rostrup-Nielsen, *J. Catal.*, 1985, **96**(2), 517–534.

76 S. Ashihara, *Ensemble*, 2009, **11**(2), 20–24.

77 G. Jacobs, L. Williams, U. Graham, G. A. Thomas, D. E. Sparks and B. H. Davis, *Appl. Catal., A*, 2003, **252**(1), 107–118.

78 R. Manabe, S. Ø. Stub, T. Norby and Y. Sekine, *Solid State Commun.*, 2018, **270**, 45–49.

79 S. Ø. Stub, E. Vøllestad and T. Norby, *J. Mater. Chem. A*, 2018, **6**, 8265–8270.

80 I. G. Tredici, F. Maglia, C. Ferrara, P. Mustarelli and U. Anselmi-Tamburini, *Adv. Funct. Mater.*, 2014, **24**, 5137–5146.

81 B. Scherrer, M. V. F. Schlupp, D. Stender, J. Martynczuk, J. G. Grolig, H. Ma, P. Kocher, T. Lippert, M. Prestat and L. J. Gauckler, *Adv. Funct. Mater.*, 2013, **23**, 1957–1964.

82 S. Miyoshi, Y. Akao, N. Kuwata, J. Kawamura, Y. Oyama, T. Yagi and S. Yamaguchi, *Chem. Mater.*, 2014, **26**, 5194–5200.

83 S. Ø. Stub, E. Vøllestad and T. Norby, *J. Phys. Chem. C*, 2017, **121**, 12817–12825.

84 C. Tandé, D. Pérez-Coll and G. C. Mather, *J. Mater. Chem.*, 2012, **22**, 11208–11213.

85 S. Ø. Stub, K. Thorshaug, P. M. Rørvik, T. Norby and E. Vøllestad, *Phys. Chem. Chem. Phys.*, 2018, **20**, 15653–15660.

86 M. Takayanagi, T. Tsuchiya, K. Kawamura, M. Minohara, K. Horiba, H. Kumigashira and T. Higuchi, *Solid State Ionics*, 2017, **311**, 46–51.

87 S. Raz, K. Sasaki, J. Maier and I. Riess, *Solid State Ionics*, 2001, **143**, 181–204.

88 S. Miyoshi, Y. Akao, N. Kuwata, J. Kawamura, Y. Oyama, T. Yagi and S. Yamaguchi, *Solid State Ionics*, 2012, **207**, 21–28.

89 G. Gregori, M. Shirpour and J. Maier, *Adv. Funct. Mater.*, 2013, **23**, 5861–5867.

90 A. Takahashi, R. Inagaki, M. Torimoto, Y. Hisai, T. Matsuda, Q. Ma, J. G. Seo, T. Higo, H. Tsuneki, S. Ogo, T. Norby and Y. Sekine, *RSC Adv.*, 2020, **10**, 14487–14492.

91 C. Li and Q. Xin, *J. Phys. Chem.*, 1992, **96**(19), 7714–7718.

92 K. B. Wiberg, *Chem. Rev.*, 1955, **55**(4), 713–743.

93 B. N. Kerkeni and D. C. Clary, *Phys. Chem. Chem. Phys.*, 2006, **8**(8), 917–925.

94 M. J. Kurylo, G. A. Hollinden and R. B. Timmons, *J. Chem. Phys.*, 1970, **52**(4), 1773–1781.

95 G. C. Schatz, A. F. Wagner and T. H. Dunning, *J. Phys. Chem.*, 1984, **88**(2), 221–232.

96 M. C. J. Bradford and M. A. Vannice, *Catal. Rev.*, 1999, **41**(1), 1–42.

97 M. S. Fan, A. Z. Abdullah and S. Bhatia, *ChemCatChem*, 2009, **1**(2), 192–208.

98 Y. C. Gao, J. G. Jiang, Y. Meng, F. Yan and A. Aihemaiti, *Energy Convers. Manage.*, 2018, **171**, 133–155.

99 Y. Wang, L. Yao, S. H. Wang, D. H. Mao and C. W. Hu, *Fuel Process. Technol.*, 2018, **169**, 199–206.

100 G. Zhang, J. Liu, Y. Xu and Y. Sun, *Int. J. Hydrogen Energy*, 2018, **43**(32), 15030–15054.

101 J. Baltrusaitis and W. L. Luyben, *ACS Sustainable Chem. Eng.*, 2015, **3**(9), 2100–2111.

102 M. M. B. Noureldin, N. O. Elbashir, K. J. Gabriel and M. M. El-Halwagi, *ACS Sustainable Chem. Eng.*, 2015, **3**(4), 625–636.

103 P. Zhang, J. Tong and K. Huang, *ACS Sustainable Chem. Eng.*, 2016, **4**(12), 7056–7065.

104 S. Afzal, D. Sengupta, A. Sarkar, M. El-Halwagi and N. Elbashir, *ACS Sustainable Chem. Eng.*, 2018, **6**(6), 7532–7544.

105 S. Shoji, X. B. Peng, T. Imai, P. S. M. Kumar, K. Higuchi, Y. Yamamoto, T. Tokunaga, S. Arai, S. Ueda, A. Hashimoto, N. Tsubaki, M. Miyauchi, T. Fujita and H. Abe, *Chem. Sci.*, 2019, **10**(13), 3701–3705.

106 M. Li and A. C. van Veen, *Appl. Catal., B*, 2018, **237**, 641–648.

107 T. Oguri, K. Sugiura, T. Yabe, S. Ogo and Y. Sekine, *J. Jpn. Pet. Inst.*, 2017, **60**(5), 232–240.

108 P. C. Rieke and N. E. Vanderborgh, *J. Membr. Sci.*, 1987, **32**(2–3), 313–328.

109 G. Alberti, M. Casciola, L. Massinelli and B. Bauer, *J. Membr. Sci.*, 2001, **185**(1), 73–81.

110 B. Scherrer, M. V. F. Schlupp, D. Stender, J. Martynczuk, J. G. Grolig, H. Ma, P. Kocher, T. Lippert, M. Prestat and L. J. Gauckler, *Adv. Funct. Mater.*, 2013, **23**(15), 1957–1964.

111 P. M. Guyon, W. A. Chupka and J. Berkowitz, *J. Chem. Phys.*, 1976, **64**(4), 1419–1436.

112 M. D. Fenn and E. Spinner, *J. Phys. Chem.*, 1984, **88**(18), 3993–3997.

113 T. Y. Cheng and R. M. Bullock, *J. Am. Chem. Soc.*, 1999, **121**(13), 3150–3155.

114 D. G. Churchill, K. E. Janak, J. S. Wittenberg and G. Parkin, *J. Am. Chem. Soc.*, 2003, **125**(5), 1403–1420.

115 G. Jacobs, S. Khalid, P. M. Patterson, D. E. Sparks and B. H. Davis, *Appl. Catal., A*, 2004, **268**(1–2), 255–266.

116 G. Parkin, *Acc. Chem. Res.*, 2009, **42**(2), 315–325.

117 T. Utaka, K. Sekizawa and K. Eguchi, *Appl. Catal., A*, 2000, **194**, 21–26.

118 H. A. Gasteiger, N. Markovic, P. N. Ross and E. J. Cairns, *J. Phys. Chem.*, 1994, **98**(2), 617–625.

119 V. M. Schmidt, P. Brockerhoff, B. Hohlein, R. Menzer and U. Stimming, *J. Power Sources*, 1994, **49**(1–3), 299–313.

120 F. Alhumaidan, D. Cresswell and A. Garforth, *Energy Fuels*, 2011, **25**(10), 4217–4234.

121 D. Teichmann, K. Stark, K. Muller, G. Zottl, P. Wasserscheid and W. Arlt, *Energy Environ. Sci.*, 2012, **5**(10), 9044–9054.

122 G. W. H. Scherer and E. Newson, *Int. J. Hydrogen Energy*, 1998, **23**(1), 19–25.

123 G. W. H. Scherer, E. Newson and A. Wokaun, *Int. J. Hydrogen Energy*, 1999, **24**(12), 1157–1169.

124 B. Kerkeni and D. C. Clary, *J. Phys. Chem. A*, 2004, **108**(41), 8966–8972.